

Feedback-based Mechanical Haldane Model

Lea Sirota,¹ Roni Ilan,¹ Yair Shokef,^{2,3,4} and Yoav Lahini¹

¹*Raymond and Beverly Sackler School of Physics and Astronomy, Tel Aviv University, Tel Aviv 69978, Israel*

²*School of Mechanical Engineering, Tel Aviv University, Tel-Aviv 69978, Israel*

³*Sackler Center for Computational Molecular and Materials Science, Tel Aviv University, Tel Aviv 69978, Israel*

⁴*Center for Nonlinear Studies, Los Alamos National Laboratory, Los Alamos, NM 87545, USA*

We propose a realization of the Haldane model using active mechanical metamaterials. The Haldane model employs complex valued bonds to break time reversal symmetry in a two-band quantum system. An analogous two-band mechanical system, i.e. a bipartite lattice with one degree of freedom per lattice site implies complex valued directional couplings between the sites, which is inconsistent with Newtonian dynamics. Here we subject a conventional mass-spring lattice to external forces that are processed through a closed loop electronic controller, which is pre-programmed to generate the desired couplings in real-time. The resulting metamaterial acts as an active medium for acoustic waves, and supports strictly unidirectional mechanical wave propagation along its boundaries. Our feedback-based approach opens a new direction of autonomous programmed metamaterials that can create arbitrary lattice parameters on the same platform, including non-local and nonlinear couplings, time dependent potentials and more.

The discovery of topologically protected wave phenomena in quantum physics [1–4] with their exceptional immunity to back-scattering has recently inspired the search for analogies in classical systems, substituting the electronic band structure with acoustic dispersion relations. As systems governed by Newtonian dynamics do not naturally exhibit topological phenomena by classical waves (e.g. acoustic or elastic waves), artificially designing a material in order to shape its dispersion relation is required. This became available with the notion of engineered materials, or metamaterials [5–8]. Indeed, numerous realizations of metamaterials supporting topologically protected wave propagation have been reported over the last decade in photonics [9–11], acoustics [12–15], and mechanics [16–20].

The particular quantum topological effect that is being considered for the classical analogy plays a very important role. The Quantum Spin Hall Effect [3, 4] or the Quantum Valley Hall Effect [21], which are based on breaking spatial symmetry in a lattice and support bi-directional edge waves are the natural path to classical analogies, as they can be implemented with purely passive mechanical components. Indeed, the vast majority of reports implement these effects e.g. by designing the spacing of steel bars [14] and bottle-like Helmholtz resonators [15] in an acoustic waveguide, the spacing of resonators on a plate [18], the spring constants in a mass-spring lattice [22], a pendulum array with sophisticated couplings [16], to name a few. On the other hand, implementing analogy of the Quantum Hall Effect, i.e. a Chern insulator, which requires breaking time reversal symmetry (TRS), is considerably more involved, as passive design becomes insufficient, and consequently there have been only few associated reports; focusing on mechanical and acoustic systems, a Chern insulator was emulated in [19, 20] by attaching gyroscopes to a mass-spring lattice, whereas the same was achieved in [12] with circulating fluids. These methods of TRS breaking have one principle in common: they require *in-plane* degrees of freedom (DOFs) in two-dimensional systems, i.e. actual physical in-plane rotation of masses or fluids,

which results in a four-band dispersion diagram. However, it would be advantageous to break TRS via out-of-plane DOFs alone, i.e. one DOF per mass, due to several reasons: first, it will enable reproduction of quantum effects that are associated with two-band systems, such as the Haldane model [2]. Second, it appears more feasible to realize such systems experimentally, as out-of-plane DOFs imply a scalar field, such as acoustic pressure or transverse plate deflection. However, when only out-of-plane DOFs are allowed, breaking TRS in classical systems requires lattice couplings that are inconsistent with classical physics laws, including complex-valued directional, or non-reciprocal couplings, as discussed below.

In this Letter we present a method of breaking TRS in mechanical systems using only *out-of-plane* DOFs, with two DOFs per unit cell in a discrete lattice. We employ a feedback-based design, which includes application of external control forces to the masses in the out-of-plane direction, and operating the forces in real time according to a target feedback control scheme. Employing active control in the design of metamaterials has recently attracted considerable interest [23–28]. In particular, the effect of this design in emulating quantum topological phenomena is being explored [29–35]. In our system, an autonomous pre-programmed controller in each unit cell receives measurements of displacements and velocities of masses in neighboring lattice sites, processes them and feeds back to the control forces. The control operation therefore determines, in real-time, the dynamic response of the masses. Since the particular couplings are solely defined by the algorithm that we program into the controller, the feedback-based metamaterial is able to sustain any couplings (within hardware limitations), including those that are otherwise physically not achievable, such as directional or non-reciprocal couplings. Furthermore, a single system is not limited to emulate a particular quantum effect, but can be programmed to any other functionality.

We analytically and numerically demonstrate our feedback-based design method by realizing an exact mechanical implementation of the quantum Haldane Model [2]. This rev-

olutionary model proved that the Quantum Hall Effect can be obtained without an external magnetic field, but rather by breaking TRS. The Haldane model comprises two interlacing triangular sub-lattices with principal lattice vectors $\{\mathbf{a}_1, \mathbf{a}_2\}$, exhibiting two sites per unit cell, A and B , as illustrated in Fig. 1(a). In our classical mechanical implementation the circles are identical masses m_0 that can vibrate only along the vertical axis \mathbf{a}_3 . We denote the lattice constant by a . The grey bars indicate nearest neighbor couplings, which are equivalent to Hookean springs of constant $t_1 > 0$ connecting the masses. When only the t_1 springs exist, the lattice is analogous to Graphene.

The quantum Haldane Model assumes additional next nearest neighbor bonds of a complex strength $t_2 e^{\pm i\phi}$ in the directions $\mathbf{v}_1, \mathbf{v}_2, \mathbf{v}_3$, indicated by the dashed black lines in Fig. 1(a). In a mechanical context, such a bond represent a *non-reciprocal* coupling, $t_2 e^{+i\phi}$ (red arrow) towards one mass and $t_2 e^{-i\phi}$ (blue arrow) towards the other connected mass, which violates Newton's third law and is therefore non-physical. Such couplings cannot be implemented neither with passive devices such as springs, lever arms etc., nor with active devices like gyroscopes that rely on in-plane DOFs. We realize these couplings using active closed loop control. Unlike what might seem, the complex value is not a non-physical property, though, as in the time harmonic regime it relates to a velocity rather than to displacement. The full form of the Haldane Model is captured by the Bloch Hamiltonian $H(\mathbf{k}) = \sum_{l=0}^3 \mathcal{H}_l(\mathbf{k}) \sigma_l$, where \mathbf{k} is the wave vector, σ_l are the Pauli matrices, and

$$\begin{aligned} \mathcal{H}_0 &= \beta + 2t_2 \cos \phi \sum_{m=1}^3 \cos(\mathbf{k} \cdot \mathbf{v}_m), \\ \mathcal{H}_1 &= -t_1 (1 + \cos(\mathbf{k} \cdot \mathbf{a}_1) + \cos(\mathbf{k} \cdot \mathbf{a}_2)), \\ \mathcal{H}_2 &= t_1 (\sin(\mathbf{k} \cdot \mathbf{a}_1) + \sin(\mathbf{k} \cdot \mathbf{a}_2)), \\ \mathcal{H}_3 &= M - 2t_2 \sin \phi \sum_{m=1}^3 \sin(\mathbf{k} \cdot \mathbf{v}_m). \end{aligned} \quad (1)$$

In a quantum system, $\beta = 0$. In the classical-mechanical analogy of Graphene $\beta = 3t_1$, indicating the restoring t_1 force from the three nearest neighbor springs, and is not related to Haldane's next nearest neighbors bonds. The constant M accounts for a possible spatial inversion symmetry breaking in addition to the TRS breaking provided by the t_2 bonds. The goal of our embedded control system is to create a classical-mechanical metamaterial, whose Newtonian dynamics in lattice momentum space \mathbf{k} is given by

$$\omega^2 \mathbf{p}(\mathbf{k}) = H(\mathbf{k}) \mathbf{p}(\mathbf{k}), \quad (2)$$

where $H(\mathbf{k})$ is the Bloch Hamiltonian of the Haldane model, and $\mathbf{p}(\mathbf{k})$ is the complex amplitude vector of the A and B sites in momentum space. Our starting point is the Graphene-like lattice (t_1 springs only), in which we denote the DOFs of each $\{i, j\}$ unit cell by $\mathbf{u}_{i,j}(t) = (u_{i,j}^A(t), u_{i,j}^B(t))^T$. The time domain unit cell dynamics, including external mechanical control forces $f_{i,j}^A, f_{i,j}^B$ that are applied to the masses in the

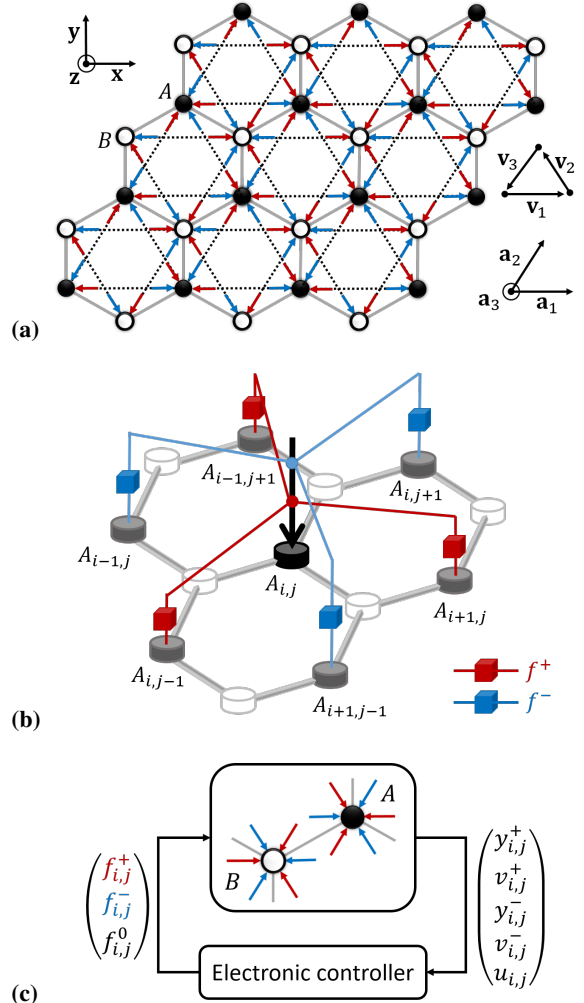


FIG. 1. Feedback control scheme for generating the exact Haldane Model in a mechanical metamaterial. (a) A honeycomb lattice in the $\{\mathbf{a}_1, \mathbf{a}_2\}$ space comprising identical masses (black and white circles) connected to nearest neighbors by Hookean springs (grey bars). The masses can move in the \mathbf{a}_3 (out-of-plane) direction only, implying two DOFs per unit cell of A and B sites. The red and blue arrows indicate out-of-plane displacement and velocity measurements of the next nearest neighbors (in $\{\mathbf{v}_1, \mathbf{v}_2, \mathbf{v}_3\}$ directions). Dashed lines indicate the Haldane model bonds that are created in real-time when control is turned on. (b) The measurement scheme detailed for the A site in the $\{i, j\}$ unit cell. The black arrow indicates the total control force $f^A = f^+ + f^- + f^0$. Red and blue arrows distinguish between measurements that are fed to controller gains $t_2 e^{+i\phi}$ and $t_2 e^{-i\phi}$ (red and blue cubes in the figure), applied through the f^+ and f^- components, respectively. (c) Feedback control scheme of the entire $\{i, j\}$ unit cell, including all the measured signals.

a_3 direction, reads

$$\begin{aligned} \ddot{u}_{i,j}^A &= 3t_1 u_{i,j}^A - t_1 (u_{i,j}^B + u_{i+1,j}^B + u_{i,j+1}^B) + f_{i,j}^A, \\ \ddot{u}_{i,j}^B &= 3t_1 u_{i,j}^B - t_1 (u_{i,j}^A + u_{i-1,j}^A + u_{i,j-1}^A) + f_{i,j}^B. \end{aligned} \quad (3)$$

The control forces are decomposed into $f_{i,j}^A = f_{i,j}^{A+} + f_{i,j}^{A-} + f_{i,j}^{A0}$ and $f_{i,j}^B = f_{i,j}^{B+} + f_{i,j}^{B-} + f_{i,j}^{B0}$. The f^+ and f^- components are responsible for generating the $t_2 e^{+i\phi}$ and the

$t_2 e^{-i\phi}$ couplings, respectively. f^0 is responsible for generating M . As depicted in Fig. 1(b), e.g. for the A site, the f^{A+} and f^{A-} components receive measured signals of displacements and velocities of the $u_{i+1,j}^A, u_{i-1,j+1}^A, u_{i,j-1}^A$ and $u_{i-1,j}^A, u_{i+1,j-1}^A, u_{i,j+1}^A$ DOFs, as indicated by the red and blue arrows, respectively. These arrows are also shown on the multi-cell lattice segment in Fig. 1(a). The f^{A0} component is not depicted in the figure. The measurements are processed in real-time by corresponding controllers, indicated by red and blue cubes. The control action is illustrated in Fig. 1(c) for the $\{i, j\}$ unit cell. For each site A and B (the superscripts are omitted in the following), the control forces are related to the measured signals as

$$(f_{i,j}^+ f_{i,j}^- f_{i,j}^0)^T = C (y_{i,j}^+ v_{i,j}^+ y_{i,j}^- v_{i,j}^- u_{i,j})^T, \quad (4)$$

where

$$\begin{aligned} y_{i,j}^+ &= u_{i+1,j} + u_{i-1,j+1} + u_{i,j-1}, \\ v_{i,j}^+ &= \dot{u}_{i+1,j} + \dot{u}_{i-1,j+1} + \dot{u}_{i,j-1}, \\ y_{i,j}^- &= u_{i-1,j} + u_{i+1,j-1} + u_{i,j+1}, \\ v_{i,j}^- &= \dot{u}_{i-1,j} + \dot{u}_{i+1,j-1} + \dot{u}_{i,j+1}. \end{aligned} \quad (5)$$

The control matrix C at each $\{i, j\}$ unit cell is given by

$$C = \begin{pmatrix} t_2 \cos \phi & \frac{t_2}{\omega} \sin \phi & 0 & 0 & 0 \\ 0 & 0 & t_2 \cos \phi & -\frac{t_2}{\omega} \sin \phi & 0 \\ 0 & 0 & 0 & 0 & \pm M \end{pmatrix}, \quad (6)$$

where the sign of M in (6) is positive (negative) for the A (B) sites. Since in frequency domain, the velocity v is related to the displacement u as $v = i\omega u$, the velocity coupling controllers are compensated by the actuation signal frequency ω . The resulting time domain evolution of the control forces generates the next nearest neighbors complex non-reciprocal bonds that are required in the Haldane Model Hamiltonian (1). This closed loop system is internally stable and the control signals amplitudes do not exceed the input signal amplitude.

Since a two-band system implies a scalar dynamical field, it significantly reduces the complexity of experimental realization compared to higher-band systems. For example, the out-of-plane displacement may be realized by an acoustic pressure field, created by a two-dimensional array of small loudspeakers. The feedback control system in (3)-(6) can be then realized by equipping each speaker with an autonomous microcontroller (which is essentially a small electronic chip [36]) that processes the pressure measured by microphones at corresponding next nearest neighbor locations.

Next we demonstrate that the mechanical system (2) governed by the classical analogy of the Haldane Model Hamiltonian (1), which we created with the control system (4)-(6), reproduces all the known dynamic properties of the quantum Haldane Model. This is not obvious a-priori, since (1) differs from the quantum Hamiltonian in its σ_0 term, and the complex valued couplings are reached only with the convergence of the control loops.

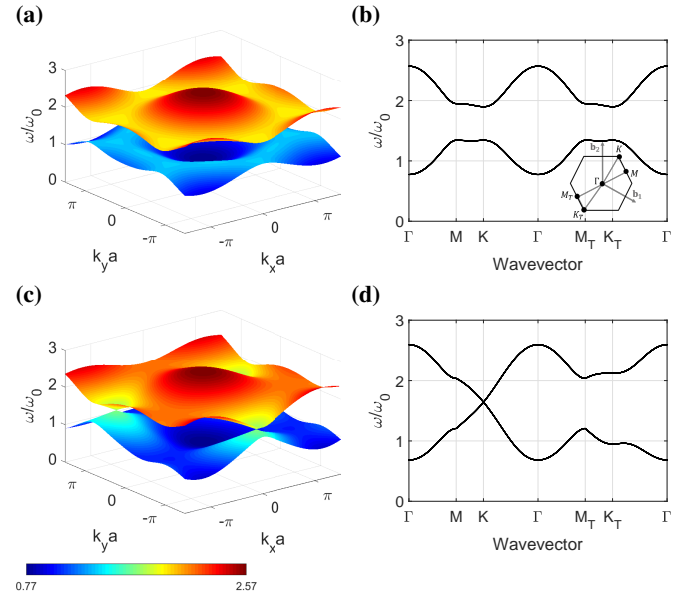


FIG. 2. Infinite lattice dispersion relations of the Haldane model mechanical analogy. The frequency scale is normalized by $\omega_0 = \sqrt{t_1/m_0}$. Dispersion diagram is plotted over the entire Brillouin zone (a),(b) and through the high symmetry points (c),(d). (a),(b) Case 1 with parameters $\{t_2 = 0.2t_1, \phi = \pi/3, M = 0\}$. (c),(d) Case 2 with parameters $\{t_2 = 0.2t_1, \phi = \pi/3, M = 3\sqrt{3}t_2 \sin \phi\}$.

The first property that we analyze is the band structure, here acoustic dispersion, of an infinite-periodic lattice. Since (2) represents a classical-mechanical system, whose dynamics is described by Newtonian equations of motion, the eigenvalues are squared frequencies. The frequencies are kept real and positive due to the constant shift of the dispersion curves by the addition of $\beta = 3t_1$ to the σ_0 term in (1). Since this addition does not change the eigenvectors, the topological properties of the original quantum Haldane Model are preserved. We consider two combinations of ϕ and M : $\{\phi = \pi/3, M = 0\}$ in case 1, and $\{\phi = \pi/3, M = 3\sqrt{3}t_2 \sin \phi\}$ in case 2. In both cases $t_2 = 0.2t_1$. The corresponding band structures of these two cases are depicted in Fig. 2. The frequency scale is normalized by $\omega_0 = \sqrt{t_1/m_0}$. Case 1 falls within the non-trivial topological regime of Chern number $n = +1$ [2]. Similarly to the quantum system, the figure shows a gap at K_T but not at K . Due to TRS breaking, the band structure is not symmetric between the $\Gamma - M - K - \Gamma$ and the $\Gamma - M_T - K_T - \Gamma$ trajectories. Case 2 falls exactly on the border between the topologically trivial ($n = 0$) and nontrivial ($n = +1$) regimes. Due to TRS breaking, a gap is opened at the K point but not at the K_T point (for $M = -3\sqrt{3}t_2 \sin \phi$ it is the other way around with $n = -1$).

Next we verify that our feedback-based topological metamaterial reproduces the edge mode dispersion of the quantum Haldane model. We consider a lattice that is infinite in the x direction and finite in the y direction, with parameters $\{t_2 = 0.2t_1, \phi = \pi/3, M = 0\}$. The dispersion diagram of an eight honeycomb cells strip is plotted in Fig. 3(a). As expected for a Chern insulator, an edge mode emerges inside

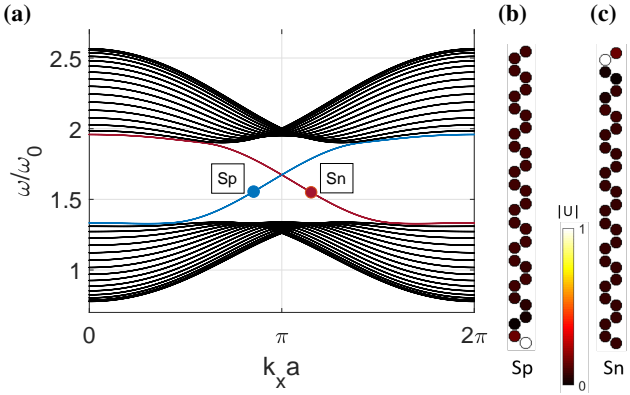


FIG. 3. Edge modes of the mechanical Haldane model. (a) Dispersion diagram of a lattice infinite in the x direction and of eight honeycomb cells in the y direction, with parameters of Case 1, $\{t_2 = 0.2t_1, \phi = \pi/3, M = 0\}$. The frequency scale is normalized by $\omega_0 = \sqrt{t_1/m_0}$. Black lines indicate bulk states. The red (blue) line indicates top (bottom) edge state with negative (positive) group velocity. (b),(c) Corresponding eigenmodes of the top and bottom edge states.

the bulk bandgap, corresponding to top edge propagation with negative group velocity (S_n point) and to bottom edge propagation with positive group velocity (S_p point). The associated eigenmodes are depicted in Fig. 3(b),(c). The wave localization on the lattice edge is guaranteed by the topological property of the band-structure.

We now demonstrate that the feedback-based mechanical Haldane Chern insulator indeed supports uni-directional edge wave propagation. We perform time domain simulations of a finite size metamaterial (8×30 honeycomb net), which is operated in a real-time feedback loop according to (2)-(6). The simulation results are given in Fig. 4. Open boundary conditions are assumed. The system is excited by a time-harmonic force $F(t) = F_0 e^{i\omega t}$ in the \mathbf{a}_3 direction at the middle of the top lattice edge, indicated by a blue arrow in the figure. The actuation frequency $\omega = 1.55\omega_0$ lies inside the bulk bandgap in Fig. 3(a) and corresponds to the point S_n there. The parameters are set to $\{t_2 = 0.2t_1, \phi = \pi/3, M = 0\}$. Closed loop time responses of the masses out-of-plane displacements $u_{i,j}(t)$ (normalized by F_0) are shown at different normalized time instances $\hat{T} = T/T_0$ with $T_0 = \sqrt{m_0/t_1}$. One clearly sees that a wave propagates along the lattice edges strictly in the counterclockwise direction, i.e. with a negative group velocity, as expected for the top edge mode. Due to topological protection, the wave circumvents the sharp lattice corners without any back-scattering.

To summarize, we demonstrated an analogy of a two-band Chern insulator, specifically the quantum Haldane model, in a classical mechanical metamaterial. Such a model requires complex valued directional couplings between masses, where only out-of-plane DOFs are allowed. As this two-band system implies a scalar field, it is much more feasible for experimental realization (e.g. with acoustic pressure field) compared to higher-band systems. However, the non-physical couplings

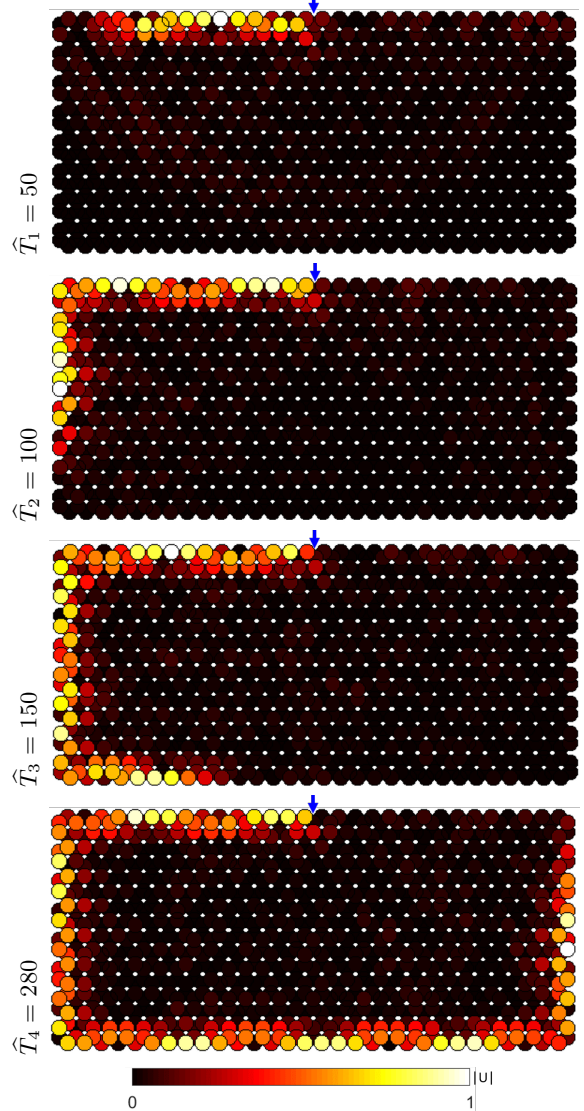


FIG. 4. Time domain simulation of the mechanical Haldane Chern insulator defined by (4)-(6) with Case 1 parameters $\{t_2 = 0.2t_1, \phi = \pi/3, M = 0\}$. A time harmonic force excitation $F(t) = F_0 e^{i\omega t}$, indicated by a blue arrow, is applied to a 8×30 honeycomb lattice in the \mathbf{a}_3 direction. The displacement responses of the masses, in \mathbf{a}_3 as well, are depicted at the normalized time instances $\hat{T}_1 = 50$, $\hat{T}_2 = 100$, $\hat{T}_3 = 150$ and $\hat{T}_4 = 280$.

could not be obtained with existing devices. We employed a feedback-based design, in which these couplings were generated via real-time autonomous control of a Graphene-like lattice. External control forces were applied to the masses, based on measured displacements and velocities of next-nearest-neighbor sites. The required non-physical couplings were encoded into the entries of the controller matrix. We demonstrated that the resulting system has all the band properties of the quantum Haldane model and supports strictly uni-directional, topologically protected, wave propagation along the metamaterial edges.

Our feedback-based approach has many advantages in con-

densed matter research, as it offers generation of arbitrary couplings on a single platform only by means of changing a control program. In particular, it has the ability to break TRS with minimal number of bands, break spatial symmetry, add gain or loss, implement long range hopping or non-local interactions, correct for imperfections, reduce dissipation and to change lattice parameters in real time (faster than the acoustic waves propagation).

We thank Moshe Goldstein and Daniel Sabsovich for fruitful discussions. This research was supported in part by the Israel Science Foundation Grant No. 968/16 and by the Israeli Ministry of Science and Technology.

[1] D. J. Thouless, M. Kohmoto, M. P. Nightingale, and M. den Nijs, *Physical Review Letters* **49**, 405 (1982).

[2] F. D. M. Haldane, *Physical Review Letters* **61**, 2015 (1988).

[3] C. L. Kane and E. J. Mele, *Physical Review Letters* **95**, 226801 (2005).

[4] B. A. Bernevig, T. L. Hughes, and S.-C. Zhang, *Science* **314**, 1757 (2006).

[5] N. Liu, H. Guo, L. Fu, S. Kaiser, H. Schweizer, and H. Giessen, *Nature Materials* **7**, 31 (2008).

[6] Y. M. Seo, J. J. Park, S. H. Lee, C. M. Park, C. K. Kim, and S. H. Lee, *Journal of Applied Physics* **111**, 023504 (2012).

[7] M. Dubois, C. Shi, X. Zhu, Y. Wang, and X. Zhang, *Nature Communications* **8**, 16 (2017).

[8] H. Zhu and F. Semperlotti, *Physical Review Applied* **8**, 064031 (2017).

[9] M. C. Rechtsman, J. M. Zeuner, Y. Plotnik, Y. Lumer, D. Podolsky, F. Dreisow, S. Nolte, M. Segev, and A. Szameit, *Nature* **496**, 196 (2013).

[10] W.-J. Chen, S.-J. Jiang, X.-D. Chen, B. Zhu, L. Zhou, J.-W. Dong, and C. T. Chan, *Nature Communications* **5**, 5782 (2014).

[11] S. H. Mousavi, A. B. Khanikaev, and Z. Wang, *Nature Communications* **6**, 8682 (2015).

[12] A. B. Khanikaev, R. Fleury, S. H. Mousavi, and A. Alu, *Nature Communications* **6**, 8260 (2015).

[13] C. He, X. Ni, H. Ge, X.-C. Sun, Y.-B. Chen, M.-H. Lu, X.-P. Liu, and Y.-F. Chen, *Nature Physics* **12**, 1124 (2016).

[14] Z. Zhang, Q. Wei, Y. Cheng, T. Zhang, D. Wu, and X. Liu, *Physical Review Letters* **118**, 084303 (2017).

[15] S. Yves, R. Fleury, F. Lemoult, M. Fink, and G. Lerosey, *New Journal of Physics* **19**, 075003 (2017).

[16] R. Süsstrunk and S. D. Huber, *Science* **349**, 47 (2015).

[17] R. K. Pal and M. Ruzzene, *New Journal of Physics* **19**, 025001 (2017).

[18] R. Chaunsali, C.-W. Chen, and J. Yang, *Physical Review B* **97**, 054307 (2018).

[19] P. Wang, L. Lu, and K. Bertoldi, *Physical Review Letters* **115**, 104302 (2015).

[20] L. M. Nash, D. Kleckner, A. Read, V. Vitelli, A. M. Turner, and W. T. Irvine, *Proceedings of the National Academy of Sciences of the USA* **112**, 14495 (2015).

[21] H. Pan, Z. Li, C.-C. Liu, G. Zhu, Z. Qiao, and Y. Yao, *Physical Review Letters* **112**, 106802 (2014).

[22] Y. Zhou, P. R. Bandaru, and D. F. Sievenpiper, *New Journal of Physics* **20**, 123011 (2018).

[23] Y. Chen, G. Hu, and G. Huang, *Journal of the Mechanics and Physics of Solids* **105**, 179 (2017).

[24] B.-I. Popa, D. Shinde, A. Konneker, and S. A. Cummer, *Physical Review B* **91**, 220303 (2015).

[25] J. Cheer, S. Daley, and C. McCormick, *Smart Materials and Structures* **26**, 025032 (2017).

[26] F. Zangeneh-Nejad and R. Fleury, *Reviews in Physics* , 100031 (2019).

[27] L. Sirota, F. Semperlotti, and A. M. Annaswamy, *Mechanical Systems and Signal Processing* **123**, 117 (2019).

[28] L. Sirota and A. M. Annaswamy, Accepted for publication in *Automatica* (2020).

[29] A. Darabi, M. Collet, and M. J. Leamy, *arXiv preprint arXiv:1911.09608* (2019).

[30] E. Rivet, A. Brandstötter, K. G. Makris, H. Lissek, S. Rotter, and R. Fleury, *Nature Physics* **14**, 942 (2018).

[31] T. Hofmann, T. Helbig, F. Schindler, N. Salgo, M. Brzezińska, M. Greiter, T. Kiessling, D. Wolf, A. Vollhardt, A. Kabaši, C. H. Lee, A. Bilušić, R. Thomale, and T. Neupert, *arXiv preprint arXiv:1908.02759* (2019).

[32] C. H. Lee and R. Thomale, *Physical Review B* **99**, 201103 (2019).

[33] C. Scheibner, W. Irvine, and V. Vitelli, *arXiv preprint arXiv:2001.04969* (2020).

[34] M. I. Rosa and M. Ruzzene, *arXiv preprint arXiv:2001.01817* (2020).

[35] M. Brandenbourger, X. Locsin, E. Lerner, and C. Coulais, *Nature Communications* **10**, 18 (2019).

[36] <https://www.analog.com/en/products/aduc7020.html>.